RSC Advances

PAPER

View Article Online
View Journal | View Issue

Cite this: *RSC Adv.*, 2015, **5**, 38030

Development of voriconazole loaded large porous particles for inhalation delivery: effect of surface forces on aerosolisation performance, assessment of *in vitro* safety potential and uptake by macrophages†

Sumit Arora,[a] Rahul R. Mahajan,[a] Varun Kushwah,[a] Dipesh Baradia,[b] Ambikanandan Misra[b] and Sanyog Jain*[a]

Received 6th January 2015
Accepted 21st April 2015

DOI: 10.1039/c5ra00248f

www.rsc.org/advances

The present study investigated the development of a dry powder inhalable formulation of voriconazole (VRZ) using quality by design (QbD) principles and assessment of its suitability for administration in the lungs. VRZ loaded large porous particles (VLPP) were extensively optimised using I-optimal design investigating the four factors (polymer type, porogen concentration, drug loading and homogenisation speed) at three different levels. Formulations were evaluated for desirable critical quality attributes (CQAs) such as particle size, drug entrapment efficiency, aerodynamic performance, porosity, surface energy, *in vitro* drug release, macrophage uptake and safety. A design space satisfying all CQAs was identified only in the case of VLPP fabricated from poly-lactide polymer (PLA). Statistical analyses suggest that all the factors and their higher order interactions influenced the morphology and physical properties of VLPP. Optimised VLPP exhibited a VRZ loading of 4.85 ± 0.39%, porosity of 0.17 ± 0.02 and median volume diameter of 8.84 ± 0.12 μm, measured with laser diffraction. Moreover, their mass median aerodynamic diameter (2.85 ± 0.38 μm) and fine particle fraction (FPF) (27.3 ± 2.7%), as measured by an 8-stage Anderson Cascade Impactor, were suitable for pulmonary delivery. VLPP was found to sustain the release of VRZ for over 7 days. Increase in the surface energy of VLPP promoted enhanced aerosolisation. No cytotoxic and inflammatory (IL-8) effect was observed when A549 cells were incubated with VLPP. In addition, VLPP was large enough to evade macrophage uptake, thus prolonging the residence time of VLPP at the site of action. Overall, this study suggests the suitability of VLPP for targeting invasive pulmonary aspergillosis by inhalation.

1. Introduction

With the increase in the complexity of modern lifestyles, there has been a significant rise in the patient population undergoing modern medical interventions and those suffering from immunosuppressive diseases such as AIDS.[1–3] Fungus, an opportunistic organism, is known to cause invasive infections in immunocompromised patients resulting in high morbidity as well as mortality. Despite such increases in incidences of invasive pulmonary fungal infections in immunocompromised patient populations, these infections are still underdiagnosed and a targeted approach to treat these infections is relatively underexplored compared with other infectious diseases.[4,5] Considering the global scenario, the patient population suffering from life-threatening fungal infections is growing at an alarming rate and finding treatment modalities to combat the menace of such infections has become a much higher priority.[4,6]

Pulmonary delivery of antifungals is increasingly gaining attention since the major route of exposure of pathogenic fungal spores is through inhalation, which is often the first step in the pathogenesis of invasive fungal infections in the lungs.[7] VRZ, a second-generation triazole antifungal agent, represents the primary salvage therapy for the treatment of invasive pulmonary aspergillosis (IPA), given either through oral or intravenous route.[3,7] However, its use is sometimes limited by excessive side effects and significant drug–drug interactions due to cytochrome P450 inhibitory potential of VRZ. Targeting of airway to deliver antifungal drugs represent a viable and

[a]*Centre for Pharmaceutical Nanotechnology, Department of Pharmaceutics, National Institute of Pharmaceutical Education and Research (NIPER), Sector 67, S.A.S. Nagar, Mohali, Punjab-160062, India. E-mail: sanyogjain@niper.ac.in; sanyogjain@rediffmail.com; Fax: +91 172-2214692; Tel: +91 172-2292055*

[b]*TIFAC-CORE in NDDS, Pharmacy Department, Faculty of Technology and Engineering, The Maharaja Sayajirao University of Baroda, Kalabhavan, Vadodara-390 001, Gujarat, India*

† Electronic supplementary information (ESI) available. See DOI: 10.1039/c5ra00248f

attractive solution to overcome this problem.[7] A number of reports on inhaled antifungals, particularly amphotericin B and itraconazole have demonstrated favourable lung retention profile, improved outcomes in animal models and probable clinical utility.[8–14] However, pulmonary delivery of VRZ has received comparatively little attention. Tolman *et al.* evaluated single and multiple dose pharmacokinetics of inhaled VRZ solution in mice and demonstrated attainment of clinically relevant therapeutic concentration.[15] In another work done by the same group, particulate formulation of VRZ prepared by thin film freezing were administered to mice and founded to attain high concentrations in the lungs as well as in plasma.[16,17] However, both the studies showed rapid clearance of VRZ from the lungs, thereby limiting its residence time.

Sinha *et al.* evaluated VRZ loaded poly-lactide-*co*-glycolide nanoparticles for delivery in the lungs. However, the formulation was optimised using conventional (one variable at a time) approach and does not take into account effect of all factors (formulation and process factors) at once on the desirable CQAs.[18]

Large porous particles fabricated from biodegradable polymers represent a suitable delivery vehicle capable of delivering drugs to the middle and lower regions of the lungs.[19,20] In addition, they also offer the advantage of escaping macrophage uptake by virtue of their large geometric size and sustaining the release of drug, thereby prolonging the residence time of encapsulated drug in the lungs.[21–23] The present investigation utilizes the QbD principles to develop a controlled release large porous microparticulate formulation fabricated from biodegradable polymers for the pulmonary delivery of VRZ. To best of our knowledge and thorough literature survey, this is the first report investigating in detail the development and characterisation of VLPP for the targeted treatment of IPA based on QbD principles. VLPP was extensive characterised in terms of physicochemical characteristics, entrapment efficiency, aerosolisation potential, surface energy, *in vitro* release of VRZ, macrophage uptake and *in vitro* safety studies to determine suitability of VLPP for lung delivery.

2. Materials and methods

2.1 Materials

Poly(D,L-lactide-*co*-glycolide) (PLGA) polymers, Resomer® RG502 (lactide : glycolide = 50 : 50), Resomer® RG752H (lactide : glycolide = 75 : 25) and poly(D,L lactide) (PLA, molecular weight 10 000–18 000, viscosity 0.16–0.24) were purchased from Boehringer Ingelheim (Ingelheim, Germany). Poly(vinyl alcohol) (PVA) with average MW 30–70 kDa and ammonium bicarbonate were purchased from Sigma (St. Louis, MO, USA). VRZ (Pharma Grade) was a kind gift from Ranbaxy Laboratories (Gurgaon, India). All other chemicals and solvents were of the highest analytical grade commercially available.

2.2 Preparation of VLPP

VLPP were prepared using a water-in-oil-in-water (w/o/w) double emulsion method.[22] Experiments were performed as per experiment design created using statistical software SAS JMP® 10 (SAS Institute Inc., Cary, USA). Briefly, PLGA or PLA and VRZ were dissolved in 3.75 mL ethyl acetate. Freshly-prepared ammonium bicarbonate solution was added to the polymer solution (w/w percent with respect to polymer) and the mixture was sonicated in ice bath using a probe sonicator (Misonix, USA) for 30 s alternating on and off (1 min total sonication time) at 25% amplitude. The sonicated mixture was added to 25 mL of 1% polyvinyl alcohol (PVA) solution while it was being homogenized at a rate of 4000–8000 rpm using a Polytron PT 4000 (Switzerland). It was then poured into 50 mL of water, and stirred for 8 h at room temperature to remove ethyl acetate. The particles were collected by centrifugation at 4000 rpm for 5 min and washed 3 times with distilled water. The suspension was then lyophilised to obtain the dry powder.

2.3 Experimental design and protocol

A I-optimal experimental design was custom built using SAS JMP® 10 (SAS Institute Inc., Cary, USA) in order to investigate the effect of various factors, *viz.* polymer type, theoretical drug loading, homogenization speed and porogen concentration (% w/w with respect to the polymer) on the formation of VLPP. Preliminary experiments (data not shown) helped in the selection of factors which were explored at three levels (as broad as possible) as mentioned in Table 1. The selection of experimental design was based on Fraction of Design Space (FDS) plot such that 90% of the experimental domain was covered with minimum variance. The software yielded a total of 24 experiments with 2 centre points to explore the experimental domain. Experiments were run in random order to increase the predictability of the model. The experimental design and the conditions are mentioned in Table 2.

Prediction model was estimated using the least squares method and is given according to the following eqn (1):

$$Y = \beta_o + \sum \beta_i X_i + \sum \beta_{ii}(X_i - \mu_i)^2 + \sum \beta_{ij}(X_i - \mu_i)(X_j - \mu_j) + \in \quad (1)$$

where Y is the predicted response, β is the parameter estimate, μ is the mean of the parameter, X is the independent parameter and $\in$ is the residual error.

Main effects, first order and second order interactions were taken into consideration for the construction of prediction

Table 1 Formulation and process factors included in the I-optimal design for the optimisation of voriconazole loaded large porous particles

Factor	Nature of factor	Levels		
		Low	Middle	High
Polymer type	Categorical	PLGA 502	PLGA 752H	PLA
Drug loading (%)	Numeric	5	10	15
Homogenisation speed (rpm)	Numeric	4000	6000	8000
Porogen concentration (% w/w)	Numeric	0	3.75	7.5

Table 2 I-optimal design for the optimisation of voriconazole loaded large porous particles

Run order	Polymer type	Drug loading (%)	Homogenisation speed (rpm)	Porogen (% w/w)
1	PLA	10	8000	7.5
2	PLGA 752H	10	4000	7.5
3	PLGA 502	15	6620	3.75
4	PLGA 502	15	4000	7.5
5	PLGA 502	10	8000	7.5
6	PLGA 752H	5	6000	0
7	PLGA 752H	15	6000	7.5
8	PLGA 502	5	8000	0
9	PLA	15	8000	0
10	PLA	10	4000	0
11	PLGA 502	5	6620	7.5
12	PLA	15	4000	7.5
13	PLGA 752H	10	8000	0
14	PLA	10	6000	3.75
15	PLGA 752H	5	8000	3.75
16	PLGA 752H	15	4000	3.75
17	PLGA 752H	5	6000	3.75
18	PLA	5	8000	7.5
19	PLGA 752H	10	6000	2.5
20	PLGA 502	5	4000	0
21	PLGA 502	10	6000	7.5
22	PLGA 502	15	4000	3.75
23	PLA	10	4000	0
24	PLA	5	8000	3.75

model. Model was accepted if it exhibited no lack of fit, no correlation in the residual plots and the residuals were normally distributed. Model was validated by selecting three check points in the design space. These points correspond to the spots in the optimality region where the model predicts desirable VLPP CQAs.

2.4 Solid state characterisation

2.4.1 Thermal analysis. Samples were subjected to thermal ramp in order to determine melting point and heat of fusion using Differential Scanning Calorimeter (DSC) (Model Q2000, TA Instruments, USA). The sample cell was purged with dry nitrogen at a flow rate of 50 mL min^{-1}. Accurately weighed samples (5 mg) in aluminium crimped pans were scanned at a heating rate of 20 °C min^{-1} over a temperature range of 35–200 °C. DSC was pre-calibrated for temperature and heat flow using high purity indium. All measurements were performed in triplicate.

2.4.2 X-ray diffraction (XRD) analysis. XRD patterns of samples were recorded at room temperature on Bruker's D8 Advance X-ray diffractometer (Karlsruhe, Germany) using Cu-Kα radiation ($\lambda = 1.54$ Å) at 35 kV, 30 mA passing through a nickel filter. Data was collected in a continuous scan mode with a step size of 0.01° and dwell time of 1 s over an angular range of 3° to 40° 2θ. Accurately weighed amount of powder was loaded in a poly-methyl methacrylate (PMMA) holder and obtained diffractograms were analysed with DIFFRAC plus EVA (version 9.0) diffraction software.

2.5 Response measurements

2.5.1 Particle sizing. Particle size of VLPP was determined by dynamic laser diffraction (Mastersizer 2000, Malvern Instruments Ltd., UK). Briefly, about 5 mg of the microparticles were suspended in 1 mL of the distilled water using vortex-mixing. This slurry was added into the sampling unit of the instrument till a laser obscuration factor of 2–6% was achieved. All samples were analysed in triplicate. The population dispersity of samples was referred as span and calculated as reported in the following eqn (2):

$$\text{Span} = \frac{d_{90} - d_{10}}{d_{50}} \times 100 \quad (2)$$

where d_{90}, d_{10}, and d_{50} are the mean diameters at the 90%, 10%, and 50% of the population distribution, respectively.

2.5.2 Density measurements and theoretical mass median aerodynamic diameter (tMMAD) determination. The poured (d_p) and tapped densities (d_t) of the powder were measured with a tapped density tester (Smart Instrument, Bombay, India). The analysis was performed according to the test for apparent volume in the European Pharmacopeia,[22] except a 10 mL glass cylinder was used due to lack of sufficient powder. VLPP was gently poured through a funnel into the glass cylinder to a volume of approximately 5 mL. The volumes were read before and after 750 taps. The density before tapping was designated as poured density and the density after tapping was designated as tapped density.

tMMAD for spherical particles was calculated by taking into consideration the geometric diameter of VLPP and the tapped density according to the eqn (3):

$$\text{tMMAD} = \sqrt{\frac{\rho}{\rho_i}} d \quad (3)$$

where d is the mean geometric diameter of VLPP, ρ is the tapped density (g cm^{-3}) and $\rho_i = 1$ g cm^{-3}.

2.5.3 *In vitro* aerosol performance. Aerodynamic particle size distribution was determined using an eight-stage Mark II Anderson Cascade Impactor (ACI). All the prepared formulations were sieved through mesh number 230 (pore diameter 63 μm) to break the agglomerates. VLPP (10 mg) was then manually loaded into hard gelatin capsule (size 3), which was put in a Rotahaler (Cipla, Gujrat, India) and split open to release the particles. Each set of VLPP was drawn through the induction port into the ACI operated at a flow rate of 60 L min^{-1} for 4 s. The amount of particles deposited at each impaction stage was determined by HPLC estimation of VRZ by washing the particles with acetonitrile. The effective cutoff aerodynamic diameter for each stage was as follows: stage 0, 8.6 μm; stage 1, 6.5 μm; stage 2, 4.4 μm; stage 3, 3.3 μm; stage 4, 2.2 μm; stage 5, 1.1 μm; stage 6, 0.54 μm; stage 7, 0.25 μm. The fine-particle fraction (FPF) was calculated as the amount of powder with an aerodynamic size <4.4 μm (particles deposited at stage 3 and lower) divided by the initial total powder loaded in the Rotahaler (10 mg; nominal dose). The cumulative mass of powder less than effective cutoff diameter as percent of total mass recovered in the ACI was plotted against the effective cutoff diameter on log-probability

graph and mass median aerodynamic diameter (AD), and geometric standard deviation (GSD) was then calculated.

2.5.4 Particle morphology. Particle morphology of the VLPPs was visualised using scanning electron microscopy (SEM Model S30400, Hitachi, USA) at 10 keV. Samples were mounted on carbon sticky tabs and gold-coated (10 nm thickness) before imaging.

The morphology of the optimised VLPP (model validation batches) was further analysed using conventional tapping mode, atomic force microscopy (AFM) (Nanoscope IIIa controller with Multimode AFM, Veeco, USA) and compared with the non-porous VRZ loaded microsphere formulation. Samples were mounted on carbon sticky tabs and imaged in air using tapping mode tips (OTESPA, Veeco, USA) at a scan rate of 0.5 Hz. Pore depth was calculated using section analysis. The surface roughness was quantified by post image analysis. Individual particles ($n \geq 5$) were analysed over an area of 1 μm × 1 μm areas and root mean square roughness was calculated using eqn (4):

$$R_{\mathrm{RMS}} = \sqrt{\frac{1}{n}\sum_{i=1}^{n} y_i^{\,2}} \quad (4)$$

where n is the number of data points in a topographical profile and y_i is the distance of asperities (i) from the centre line.

2.5.5 Drug loading efficiency. For determination of drug loading, accurately weighed (3–4 mg) VLPP was taken into eppendorf. This was followed by addition of 2 mL of acetonitrile. Eppendorf was then vortexed for 5 minutes, sonicated, centrifuged, and the supernatant was filtered. VRZ content was quantitatively measured using a validated high-pressure liquid chromatography (HPLC) analytical method in the supernatant. Practical drug loading and entrapment efficiency were calculated from eqn (5) and (6), respectively.

$$\text{Practical drug loading (\%)} = \frac{\text{Amount of drug present in microparticle}}{\text{Weight of microparticles taken}} \times 100 \quad (5)$$

$$\text{Entrapment efficiency (\%)} = \frac{\text{Actual drug loading}}{\text{Theoretical drug loading}} \times 100 \quad (6)$$

2.5.6 Contact angle and surface energy measurement of VLPP. The contact angle of different liquids on VLPP surface was measured by sessile drop method on a Drop Shape Analyzer (FTA 1000, First Ten Angstrom, Virginia, USA). VLPP were mounted on the double sided adhesive tape attached to the glass slide. Excessive VLPP powder was then removed by tapping. A liquid drop was introduced onto the substrate surface *via* a microsyringe. The advancing contact angles were measured for three probe liquids (water, ethylene glycol and diiodomethane) under ambient conditions of 25 ± 2 °C and 55 ± 5% RH. The surface free energy parameter was calculated using Lifshitz–van der Waals/acid–base approach utilizing contact angle values determined for three probe liquids.[24]

2.5.7 *In vitro* drug release. *In vitro* release behaviour of VRZ was determined only for optimised VLPP formulations utilized for DoE model validation. Optimised VLPP prepared with 3% and 5% porogen concentration (w/w with respect to polymer) were used for *in vitro* VRZ release studies. Release behavior of VRZ from VLPP was also compared with its release from non-porous microsphere as well as with raw VRZ.

An accurately weighed quantity of the optimised VLPP (5 mg) was placed in the dialysis membrane (12 kD) (Sigma Aldrich, USA) and suspended in 20 mL of the dissolution medium, phosphate buffer saline (pH 7.4, 10 mM) containing 0.1% Tween 80 in order to maintain sink conditions. At fixed intervals of time, samples (400 μL) were withdrawn and replenished with freshly prepared buffer. The samples were then analysed for the VRZ content using validated HPLC. All the experiments were performed at 37 ± 0.5 °C and 100 rpm. The cumulative percentage VRZ released was calculated, and the mean values and standard deviations were reported. The release profile of VRZ from VLPPs were further mathematically modeled to determine the release kinetics of VRZ from VLPPs.

2.6 Cell culture

Lung adenocarcinoma (A549) and murine macrophage cell line (RAW 264.7) were procured from National Centre for Cell Science (NCCS), Pune, India. A549 cells were cultured under conditions as previously described by Sanyog Jain *et al.*[25] RAW 264.7 were cultured using the air-liquid (gaseous phase) culture methods as described by Kim *et al.*[26] and Hwang *et al.*[27] with minor modifications. The macrophages obtained by these methods are expected to possess phagocytosis property similar to the primary alveolar macrophages *Φ*.[27,28] Briefly, cells were suspended at a concentration of 2–3 × 10^{-6} cells per mL in DMEM containing 10% (w/v) FBS and antibiotics. An aliquot (1 mL) of the cell suspension was seeded on a cell culture insert (Transwell®, 0.4 μm pore size, 0.33 cm^2 surface area, Corning Costar, Lowell, MA, USA), and 3 mL of medium was added to each of the 6 wells (Costars, Corning 261 Inc., NY, USA). The plates were then incubated at 37 °C in a 5% CO_2 atmosphere. After a 12 h incubation, the medium in the culture insert was removed and the cells was gently washed with PBS (200 μL) two times. Fresh DMEM containing 10% FBS was added to each well.

2.6.1 Cell viability assay. The cultured cells (A549), washed with Hank's Buffered Salt (HBS) Solution (PAA, Austria) for three times, were taken for MTT assay. After removing the HBS solution from the plates, cells were treated with increasing concentrations of VRZ (1.2 nM to 150 μM) and VLPP (1.2 nM to 15 μM) for 72 h. Cell viability was then determined by MTT assay. Briefly, cells were washed with HBS solution and incubated again with 0.2 mL fresh DMEM containing 0.5 mg mL^{-1} MTT (Sigma, USA) for 3 h. The medium was then removed and MTT formazon was dissolved in 0.2 mL dimethylsulfoxide. The optical density was then determined at 550 nm using an ELISA plate reader (BioTek, USA).

2.6.2 Inflammatory response *in vitro*. Basolateral media collected after 4 h exposure of A549 to the VRZ and VLPP (0.1,

1 and 10 μM) were analysed for interleukin-8 (IL-8) levels using an ELISA MAX kit (Biolegend, Inc., San Diego, CA, USA). Treatment with saline was used as control. Data is expressed as percentage of the control group.

2.6.3 Macrophage uptake study. Nile Red was co-encapsulated in non-porous and large porous particles for macrophage uptake studies. The dye was added in the organic phase and formulations were prepared following the optimized condition determined by design space. Fraction of VLPP deposited on stage 3 through 6 of ACI were recovered together and used for macrophage uptake study. RAW 264.7 were cultured as described earlier. The cells were incubated with recovered fractions for 3 h. The cells were observed under the confocal laser microscope (CLSM) (Olympus FV1000) before as well as after washing with HBSS (5×).

2.7 Principal component analysis and other statistical analysis

Principal Component Analysis (PCA) computed with SAS JMP® 10 was used to obtain visual overview of interactions between factors and responses. PCA reduces the complexity of the data set by introducing principal components. The first principal component (PC1) accounts for the largest variation across the experimental domain while the second principal component (PC2) orthogonal to the first component accounts for the second largest variation. Loading plot and score plot were plotted to gain useful insights in the complex data set obtained from the DoE runs. Correlation matrix was also computed in order to observe dependency of various factors and responses among one another.[29,30]

All other statistical calculations were performed with GraphPad Instat version 5.1 (GraphPad Software, Inc., San Diego California). The data were analysed either by one-way analysis of variance (between several objects) or by unpaired *t*-test (between two objects) to determine significant differences. Statistical significance was based on a probability value of less than 0.05 and in some cases 0.01.

3. Results

VLPP made from PLA exhibited desirable particle characteristics for deep lung targeting. Results of the extensive particle characterisation are mentioned in Table 3. In all the 24 experiments, white powder material was obtained. The yield was above 70% in all the experimental runs.

3.1 Design of experiments

3.1.1 Experimental domain evaluation and identification of design space. DoE helps to demonstrate how the system works as a whole when multiple factors are taken into consideration at once. 24 runs were aptly conducted according to an I-optimal design which is robust against outliers.

The prime most aim was to identify the design space within the experimental domain where all the CQAs were satisfied and the best settings could be determined to obtain the quality target product profile (QTPP). The desired CQAs were: (a) AD (between 1–5 μm) (b) FPF (>25%) (c) GSD (<5) (d) Geometric diameter (between 8–20 μm) (e) span (<5) (f) tMMAD (between 1–5 μm) (g) practical drug loading (>4%) (h) entrapment efficiency (>60%). The values of surface energy, poured density and tapped density were also determined and modelled. However, no limits were set for these factors. Keeping in considerations all these desirable attributes, the experimental domain was investigated. Interestingly, design space (depicted by white region in the Fig. 1) was obtained only in the case of PLA under the given set of experimental setting. VLPP prepared from PLA were only able to satisfy the criteria defined for the CQAs. R^2 values varying from 0.67 to 0.98 were obtained for response variables investigated following mathematical modelling (Fig. 2) (surface profilers explaining the relationship between factors and responses measurements of VLPP fabricated from PLA has been mentioned in ESI† since design space was only identified in VLPP fabricated from PLA).

3.1.2 Validation of I-optimal design for the optimisation of VLPP. Results of DoE model validation are mentioned in Table 4. The prediction error was found to be less than 10% for all the responses except in the case of span, tMMAD and geometric diameter.

3.2 Solid state characterisation of VLPP

XRD diffractogram of the VLPP fabricated from PLGA 502, PLGA 752H and PLA (Fig. 3A) showed absence of characteristic peaks of VRZ which was observed in the XRD spectra of raw VRZ. In addition, DSC (Fig. 3B) showed the absence of endotherm at 131 °C corresponding to the melting point of VRZ in all the microparticulate formulations.

3.3 Principal component analysis (PCA)

PCA is a useful statistical technique for visualizing the interactions between the factors and responses. PCA of the DoE runs helped in gaining useful insights and deriving possible correlation among various factor and responses by reducing the complexity of the data set. The principal component 1 (PC1) represented the largest variation of 33.9% which was due to homogenization speed (Fig. 4A) while principle component 2 (PC2) explained variation due to porogen concentration and accounted for 24.9% of the total variance of the data set (Fig. 4B). The third principal component accounted for 12.5% variation due to the drug loading (data not shown). All the three principal components together explain 69.6% of the total variation in the data set.

Loading plot provides more visually pleasing representation of correlation between the various response variables and process parameters. Parameters and variables grouped close to each other are positively correlated while those opposite to each other are negatively related. Parameters and variables which are perpendicular to each other does not have any influence on each other. This represented a useful way to discern relationships in the complex data generated from the DoE runs (Fig. 5).

Table 3 Observed responses measurements for the 24 experimental runs of I-optimal design[a]

DoE run	AD (μm)	FPF (%)	GSD	SPAN	tMMAD (μm)	Surface energy (mJ m^{-2})	Geometric diameter (μm)	Practical loading (%)	Entrapment efficiency (%)	Poured density (g cm^{-3})	Tapped density (g cm^{-3})	Porosity
1	4.82 (0.89)	13.25 (2.34)	2.74 (0.65)	1.60 (0.32)	2.62 (0.11)	44.76 (1.98)	6.80 (0.67)	6.00 (0.74)	60.00 (7.4)	0.109 (0.018)	0.149 (0.012)	0.272 (0.062)
2	3.28 (0.54)	25.99 (4.55)	3.23 (0.98)	7.78 (1.49)	7.36 (1.16)	53.23 (1.45)	46.00 (3.34)	3.10 (0.39)	31.00 (3.90)	0.016 (0.005)	0.026 (0.008)	0.385 (0.003)
3	3.94 (0.62)	24.04 (3.56)	3.82 (0.54)	1.30 (0.23)	2.43 (0.08)	54.24 (1.23)	10.10 (0.89)	3.20 (0.20)	21.33 (1.33)	0.047 (0.008)	0.058 (0.004)	0.193 (0.083)
4	11.06 (1.78)	19.89 (2.87)	8.10 (1.78)	6.04 (0.56)	8.69 (0.55)	49.76 (2.78)	17.62 (1.56)	3.40 (0.87)	22.67 (5.80)	0.162 (0.034)	0.244 (0.031)	0.341 (0.056)
5	4.03 (0.32)	22.00 (4.34)	5.12 (0.76)	17.67 (3.23)	4.25 (0.25)	51.40 (1.56)	11.25 (1.23)	3.05 (0.65)	30.50 (6.54)	0.104 (0.009)	0.143 (0.017)	0.271 (0.024)
6	14.01 (1.56)	21.67 (1.98)	6.94 (1.09)	55.26 (6.34)	15.88 (1.07)	54.36 (2.34)	24.00 (2.76)	1.95 (0.16)	39.00 (3.24)	0.362 (0.037)	0.439 (0.059)	0.173 (0.027)
7	5.49 (0.78)	27.75 (3.78)	3.58 (0.82)	2.54 (0.32)	6.28 (0.38)	59.87 (1.56)	28.14 (2.89)	4.90 (0.87)	32.67 (5.87)	0.028 (0.006)	0.050 (0.006)	0.444 (0.054)
8	4.26 (0.23)	23.43 (1.34)	3.82 (0.67)	1.88 (0.27)	4.77 (0.24)	52.58 (1.76)	7.80 (0.78)	1.68 (0.12)	33.60 (2.43)	0.298 (0.049)	0.375 (0.038)	0.209 (0.051)
9	2.67 (0.12)	19.48 (2.78)	2.45 (0.47)	1.24 (0.33)	1.62 (0.19)	54.65 (1.67)	3.00 (0.12)	6.13 (0.76)	40.87 (5.07)	0.248 (0.075)	0.294 (0.067)	0.167 (0.067)
10	8.92 (0.76)	14.65 (1.05)	4.70 (0.54)	1.32 (0.19)	9.70 (0.26)	47.31 (2.67)	16.29 (1.45)	5.12 (0.63)	51.20 (6.32)	0.326 (0.034)	0.355 (0.019)	0.083 (0.047)
11	7.38 (0.45)	20.71 (3.67)	7.26 (0.73)	6.04 (1.33)	5.67 (0.19)	49.94 (1.67)	15.62 (0.56)	2.42 (0.14)	48.40 (2.80)	0.091 (0.006)	0.132 (0.009)	0.311 (0.002)
12	5.39 (0.14)	26.20 (2.34)	3.61 (0.77)	8.83 (0.10)	7.75 (0.57)	52.87 (1.38)	42.08 (3.24)	5.06 (0.56)	33.73 (3.73)	0.022 (0.005)	0.034 (0.005)	0.358 (0.053)
13	6.57 (0.34)	12.85 (1.98)	3.93 (0.63)	10.95 (1.23)	2.40 (0.09)	42.08 (0.96)	3.75 (0.23)	3.94 (0.45)	39.40 (4.50)	0.384 (0.041)	0.409 (0.029)	0.063 (0.034)
14	3.44 (0.14)	25.21 (3.56)	3.44 (0.34)	3.01 (0.65)	3.81 (0.24)	57.97 (0.67)	6.84 (0.42)	4.50 (0.29)	45.00 (2.90)	0.262 (0.056)	0.310 (0.039)	0.161 (0.076)
15	16.31 (1.97)	20.04 (1.67)	8.46 (2.23)	3.53 (0.23)	16.75 (0.58)	48.23 (0.78)	33.95 (2.45)	2.56 (0.34)	51.20 (6.8)	0.181 (0.016)	0.244 (0.017)	0.259 (0.014)
16	11.34 (0.89)	18.46 (2.67)	5.16 (1.07)	3.47 (0.45)	10.61 (0.29)	49.34 (1.89)	32.00 (3.23)	2.82 (0.19)	18.80 (1.27)	0.084 (0.010)	0.110 (0.006)	0.238 (0.049)
17	7.24 (0.93)	17.70 (1.89)	3.38 (0.45)	3.91 (0.48)	6.84 (0.26)	50.35 (1.65)	16.45 (1.67)	3.45 (0.29)	69.00 (5.8)	0.138 (0.013)	0.173 (0.013)	0.203 (0.015)
18	3.24 (0.16)	24.39 (2.85)	2.19 (0.65)	16.80 (2.98)	3.74 (0.06)	58.71 (1.76)	12.61 (0.87)	4.20 (0.56)	84.00 (11.2)	0.061 (0.008)	0.088 (0.003)	0.308 (0.067)
19	18.74 (2.41)	11.45 (1.23)	5.16 (1.23)	35.25 (3.98)	24.61 (1.56)	40.53 (0.64)	40.41 (3.87)	4.30 (0.79)	43.00 (7.91)	0.327 (0.039)	0.372 (0.047)	0.120 (0.006)
20	14.35 (1.67)	8.05 (1.34)	7.10 (2.34)	2.77 (0.17)	9.49 (0.13)	40.76 (0.96)	14.46 (1.82)	2.24 (0.29)	44.80 (5.82)	0.399 (0.013)	0.431 (0.012)	0.074 (0.004)
21	9.67 (0.45)	16.45 (1.67)	9.07 (1.67)	57.72 (5.98)	9.40 (0.59)	50.91 (2.34)	24.90 (2.03)	1.38 (0.45)	13.80 (4.50)	0.097 (0.03)	0.143 (0.018)	0.332 (0.127)
22	12.25 (1.34)	15.52 (2.44)	10.84 (1.98)	2.89 (0.46)	9.74 (0.76)	46.80 (1.76)	25.99 (2.45)	1.41 (0.34)	9.40 (2.27)	0.117 (0.016)	0.141 (0.022)	0.169 (0.016)
23	7.86 (0.87)	18.94 (1.34)	7.63 (0.93)	1.65 (0.21)	7.25 (0.34)	49.64 (1.67)	11.22 (1.13)	4.70 (0.76)	47.00 (7.60)	0.406 (0.043)	0.418 (0.039)	0.029 (0.012)
24	4.21 (0.23)	29.48 (1.23)	3.86 (0.29)	2.24 (0.67)	2.67 (0.09)	57.51 (1.73)	4.86 (0.19)	3.80 (0.19)	76.00 (3.80)	0.247 (0.024)	0.303 (0.021)	0.186 (0.023)

[a] AD – aerodynamic diameter, FPF – fine particle fraction, GSD – geometric standard deviation, tMMAD – theoretical mass median aerodynamic diameter. Values in parenthesis represent S.D. ($n = 6$) except in case of AD, FPF and GSD where $n = 3$.

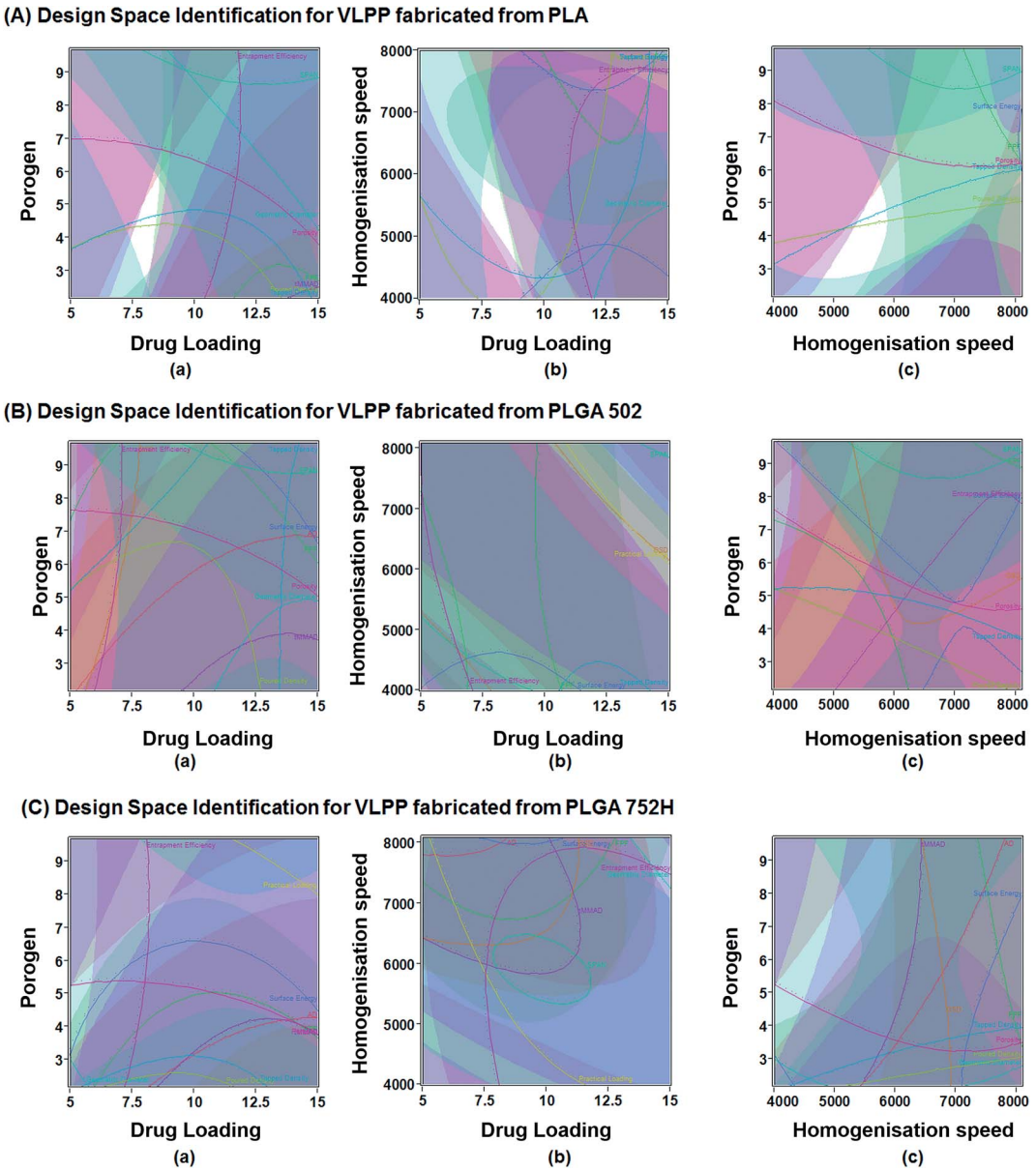

Fig. 1 Contour plots depicting design space for VLPP fabricated from (A) PLA (B) PLGA 502 and (C) PGA752H. The plots were obtained between (a) porogen and drug loading, (b) homogenization speed and drug loading and (c) porogen and homogenization. White region represents the design space in which all the desirable critical quality attributes are satisfied.

3.4 Effect of factors on response variables

3.4.1 Effect on particle morphology. Representative SEM micrographs of VLPP fabricated from PLA, PLGA 752H and PLGA 502 are shown in Fig. 6A–C respectively. In general, VLPP showed spherical shaped particles with particle size data in good agreement as that obtained by dynamic light scattering (DLS).

SEM images further revealed that the particle morphology and surface texture were greatly influenced by the porogen concentration and polymer type. In all the cases, as the concentration of ammonium bicarbonate was increased, both the pore size and pore density were found to be increased. These results were consistent with the previous published studied utilizing this porogen.[31–33] The microspheres were non-porous with 0% porogen concentration while showed highly porous structure with 7.5% porogen concentration. VLPP fabricated from PLGA 752H showed very rough surface texture at 7.5% concentration of ammonium bicarbonate.

The inherent strength of the polymeric backbone played an important role in maintaining integrity of porous microspheres. Microspheres with well-defined morphology were obtained in case of PLA at all concentrations of porogen tested while in case of PLGA 502, broken microspheres were observed at high concentration of porogen.

AFM topographical imaging of optimised VLPP (model validation batches) further helped in gaining useful information

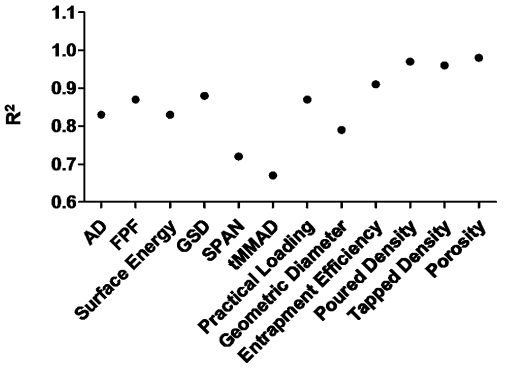

Fig. 2 Mathematical fitting of critical quality attributes following multiple regression analysis as depicted by R^2 values. AD – aerodynamic diameter, FPF – fine particle fraction, GSD – geometric standard deviation, tMMAD – theoretical mass median aerodynamic diameter.

regarding the morphology of the prepared VLPP (Fig. 7). The nanoscopic surface characteristics were further studied, pore size and surface roughness as assessed by post image analysis are reported in Table 5.

3.4.2 Effect on geometric particle size and span. The median volume diameter of VLPP determined by laser diffraction was found in the range 3–42 μm within the entire experimental domain (Table 3). The particle diameter of VLPP obtained in the design space varied between 8–13.5 μm which is generally the particle size range for large porous particles meant for inhalation delivery.

Homogenization speed and porogen concentration were the most important factors affecting the geometric particle size and span of VLPP as analysed by Pareto charts (data shown in ESI†). An increase in homogenization speed resulted in decrease in particle size of VLPP with narrower span index whereas porogen concentration exerted the opposite effect. Increase in porogen concentration resulted in VLPP with large geometric diameter and wider span (Table 3). These results are along the expected lines as documented in literature also.[32,33]

3.4.3 Effect on particle density and tMMAD. Poured density and tapped density of VLPP were mainly affected by the changes in concentration of the porogen as shown by loading plot (Fig. 5) and also analysed by Pareto charts (data shown in ESI†). Negative correlation of 0.76 and 0.8 was observed for poured and tapped density respectively in relation to the porogen concentration. Drug loading was also found to influence the density of VLPP. Two way interactions between polymer type/homogenization speed and polymer type/porogen also significantly affected the density of the formulations. tMMAD of VLPP was found to be influenced by the factors such as homogenization speed, polymer type and two-way interactions between homogenisation speed and porogen concentration.

3.4.4 Effect on aerosolisation performance (AD, FPF and GSD). Aerosolisation efficiency of the prepared VLPP were analysed in depth according to the British Pharmacopoeia for DPIs (Appendix XXI F, http://www.pharmacopeia.co.uk) and

Table 4 Validation of I-optimal design for the optimisation of voriconazole loaded large porous particles[a]

Model validation batch	Polymer type	Drug loading	Homogenization speed	Porogen	Actual by predicted	AD (μm)	FPF (%)	Surface energy (mJ m^{-2})	GSD	SPAN	tMMAD (μm)	Practical loading (%)	Geometric diameter (μm)	Entrapment efficiency (%)	Poured density (g cm^{-3})	Tapped density (g cm^{-3})	Porosity
I	PLA	8	5400	3	Predicted	3.11	25.78	55.49	2.64	2.24	3.39	4.81	8.43	61.98	0.285	0.317	0.101
					Actual	3.38	26.32	57.98	2.85	2.67	4.49	5.06	8.03	63.3	0.281	0.314	0.105
					Prediction error (%)	8.68	2.09	4.49	7.96	19.19	32.45	5.19	4.78	2.13	1.40	1.06	3.96
II	PLA	7.5	5900	4	Predicted	2.34	26.59	56.48	2.11	4.01	3.26	4.62	8.17	65.59	0.235	0.281	0.164
					Actual	2.56	27.3	59.87	1.98	4.47	4.73	4.85	8.84	64.78	0.238	0.287	0.170
					Prediction error (%)	9.41	2.63	6.01	6.16	11.47	45.09	4.98	8.02	1.23	1.28	2.14	3.53
III	PLA	8.3	5600	5	Predicted	1.78	25.4	54.78	1.73	3.12	4.67	4.77	12.7	62.87	0.198	0.267	0.258
					Actual	1.89	25.9	56.34	1.82	3.64	5.59	4.95	10.68	62.16	0.203	0.274	0.259
					Prediction error (%)	6.17	1.9	2.84	5.2	14.28	19.70	3.77	15.91	1.12	2.53	2.62	0.04

[a] Each data value in 'actual' row represents an average reading of three independent batches. AD – aerodynamic diameter, FPF – fine particle fraction, GSD – geometric standard deviation, tMMAD – theoretical mass median aerodynamic diameter.

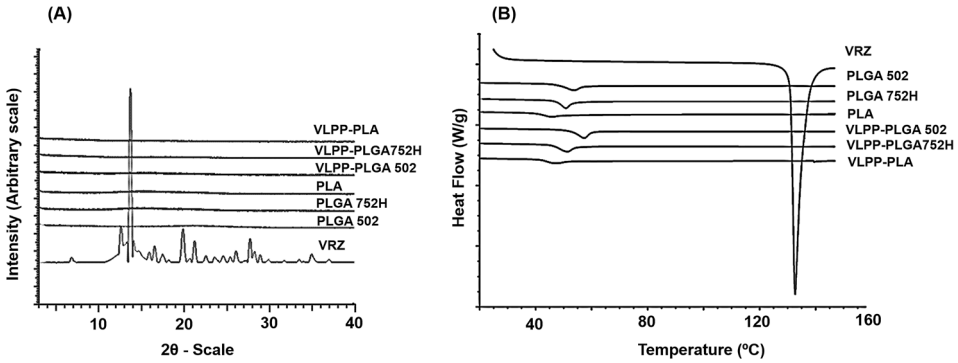

Fig. 3 Solid state characterisation of VLPP fabricated from different polymer investigated (A) PXRD and (B) DSC analysis.

results are mentioned in Table 3. The emitted dose fraction was greater than 80% in all the experimental runs. Aerodynamic characteristics of the dry powders are complex characteristics to predict as they are affected by the multitude of factors. No single factor was found predominantly responsible for affecting the aerodynamic diameter of VLPP except the porogen concentration. Porogen concentration was found to have profound effect in determining the aerodynamic diameter of VLPP. The two-way interactions between homogenisation speed and porogen concentration as well as homogenisation speed and polymer type played a noteworthy role ($p < 0.05$) in influencing the aerodynamic diameter of the prepared VLPP (Pareto chart analysis shown in ESI†). VLPP fabricated from PLA were found to possess aerodynamic diameter within the desirable range *i.e.* 1–5 μm (Table 3).

FPF of the VLPP was found to be mainly affected by the homogenization speed and higher order interactions between homogenization speed and porogen (Pareto chart analysis shown in ESI†). VLPP formulated from PLA were found to show greater FPF (>25% of their dose) as compared to VLPP fabricated from PLGA 502 or PLGA 752H. Homogenization speed and polymer type and their higher order interactions were found to influence GSD of the VLPP. High homogenization speed led to the narrow GSD of the VLPP (Table 3).

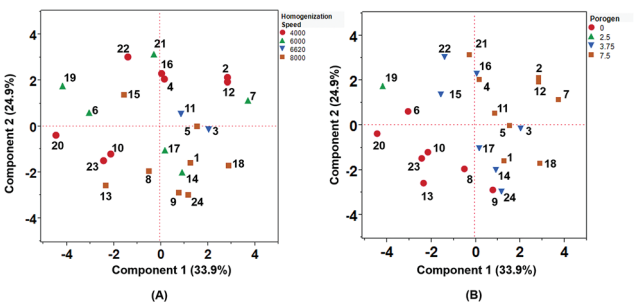

Fig. 4 Score plot from the principal component analysis with PC1 on the horizontal and PC2 on the vertical axis. Each experiment is placed according to the influence of PC1 and PC2. The ellipse indicates a 95% confidence interval. (A) Score plot labelled according to the homogenization speed (B) score plot labelled according to porogen concentration.

3.4.5 Effect on VRZ loading efficiency. Polymer type and theoretical drug loading were the predominant factors (Pareto chart analysis shown in ESI†) which influenced the entrapment efficiency and thus, actual loading of VRZ within the VLPP. VLPP fabricated from PLA polymer showed maximum entrapment efficiency (84%) as compared to other grades of PLGA at 5% (w/w) theoretical drug loading (Table 3). Homogenization speed was also found to influence the loading of VRZ within VLPP.

3.4.6 Role played by surface energy in determining aerosolisation performance of VLPP. Surface free energy for each of the VLPP formulation is reported in Table 3. No single factor was found to have significant effect in influencing the surface free energy of the VLPP ($p > 0.05$). Pareto chart analysis highlighted that the two way interactions between homogenisation speed and porogen concentration as well as homogenisation speed and polymer type significantly affected the surface free energy of VLPP. It was further interesting to note an appreciable linear correlation ($R^2 = 0.825$) between the FPF and the total surface free energy of VLPP (Fig. 8).

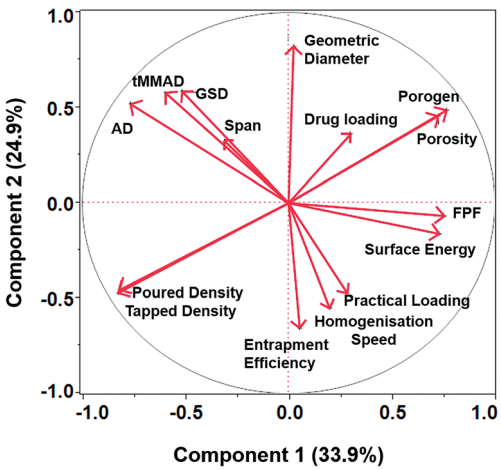

Fig. 5 Loading Plot from the principal component analysis of DoE runs with PC1 on the horizontal and PC2 on the vertical axis. AD – aerodynamic diameter, FPF – fine particle fraction, GSD – geometric standard deviation, tMMAD – theoretical mass median aerodynamic diameter.

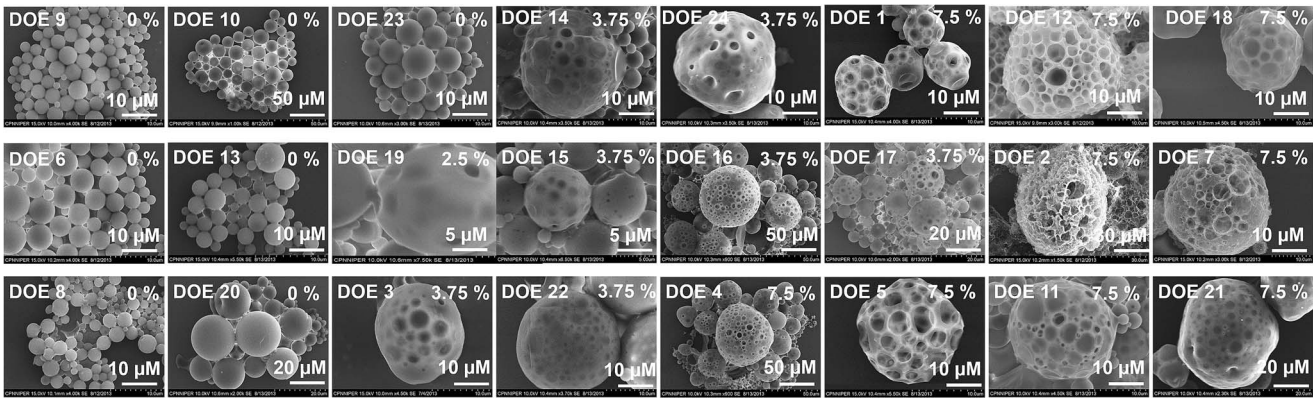

Fig. 6 Representative scanning electron microscopic images of VLPP (A) fabricated using PLA (B) fabricated using PLGA 752H and (C) fabricated using PLGA 502. The design of experiment (DoE) number and porogen concentration (% w/w with respect to polymer) used are mentioned on the upper left and upper right hand side of the photographs respectively. The scale is different for different SEM micrographs as varying sizes of microparticles ranging from 3–42 μm were obtained owing to varied processing conditions. As a result, it was not possible to accommodate all the images within same scale range.

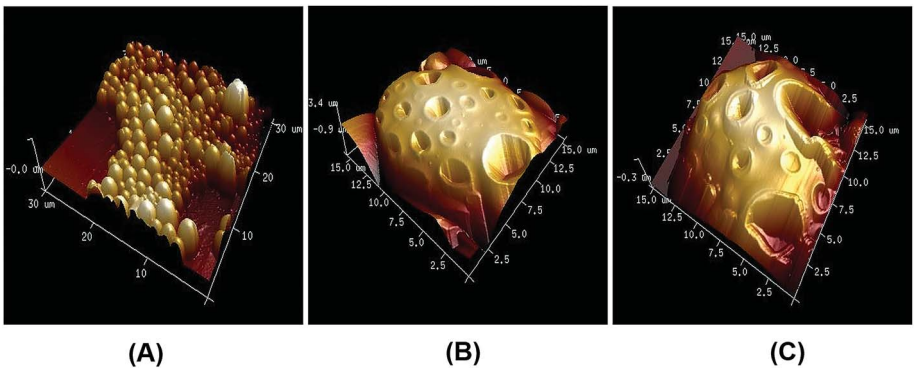

Fig. 7 AFM topographical images of optimised VLPP fabricated from PLA (A) non-porous microparticles (0% porogen concentration) (B) VLPP3 (3% porogen concentration) (C) VLPP (5% porogen concentration).

3.5 *In vitro* VRZ release from optimised VLPP batches

Fig. 9A demonstrate *in vitro* release profile of VRZ from VLPP fabricated from PLA at different porogen concentration and compared with the dissolution of free VRZ. VRZ was found to be completely released from the raw drug within 2 h and followed first order release kinetic. However, sustained release of VRZ from the VLPP was observed for a period of 7 days. VLPP prepared from 3% and 5% porogen concentration (w/w with respect to the polymer concentration) released 90.34% and 95.34% of the total VRZ loaded respectively in 7 days. Non-porous microspheres, on the other hand, released only 72.23% of the encapsulated VRZ

Table 5 Post AFM image analysis of voriconazole loaded non-porous and large porous microspheres[a]

Porous microsphere	Pore size (μm)	Surface roughness (nm)
VLPP0	—	33.22 ± 3.79
VLPP3	0.83 ± 0.24	134.18 ± 37.79***
VLPP5	1.82 ± 0.92**	349.60 ± 38.89***

[a] Each data is represented as mean ± S.D. ($n = 6$) (** $p < 0.05$, *** $p < 0.001$). VLPP0 – VLPP fabricated with zero porogen concentration (w/w with respect to polymer) VLPP3 – VLPP fabricated with 3% porogen concentration (w/w with respect to polymer) VLPP5 – VLPP fabricated with 5% porogen concentration (w/w with respect to polymer).

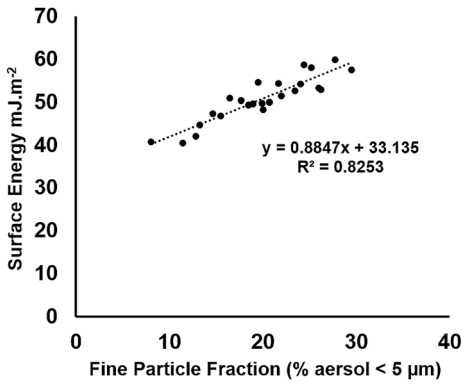

Fig. 8 Correlation between the fine particle fraction (FPF) and the total surface free energy of VLPP.

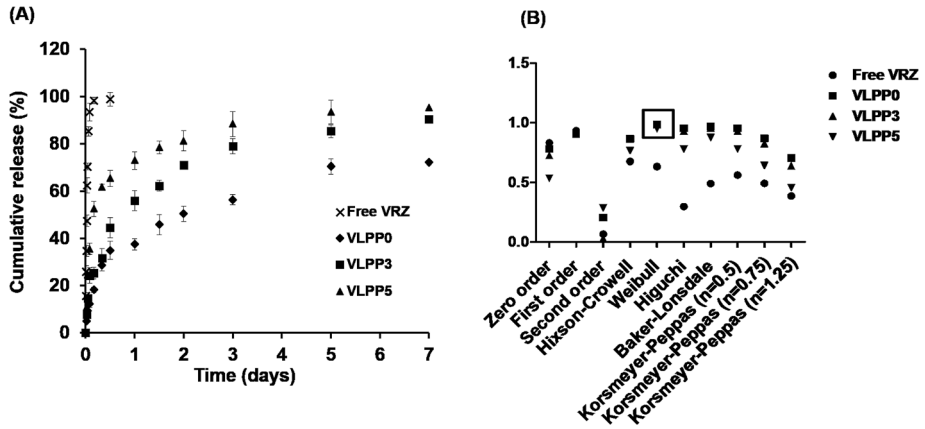

Fig. 9 (A) Cumulative release of VRZ from VLPP fabricated from PLA with 0% (VLPP0), 3% (VLPP3), and 5.0% (VLPP3) porogen concentration (w/w with respect to polymer) ($n = 6 \pm$ S.D.). (B) Mathematical modelling of release behaviour to describe the best suitable release mechanism of VRZ from VLPP.

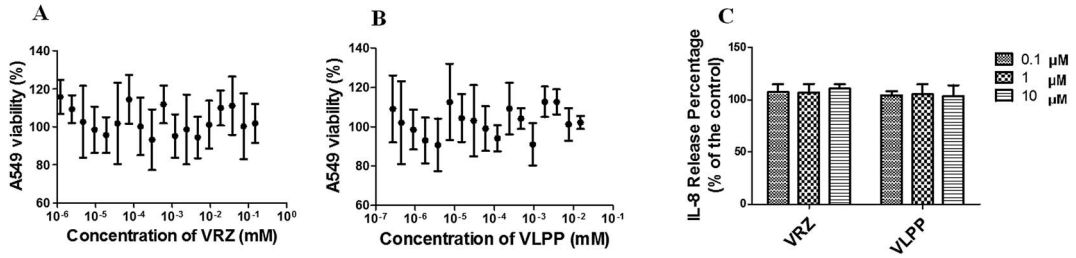

Fig. 10 The effect of (A) VRZ and (B) VLPP on A549 Cell viability following 72 h treatment ($n = 3$; mean ± StDev). (C) The release of IL-8 in cell culture media of A549 cells after exposed to different concentrations of VRZ and VLPP ($n = 3$; mean ± StDev). Values were expressed as percentage of the control group, which were treated with saline.

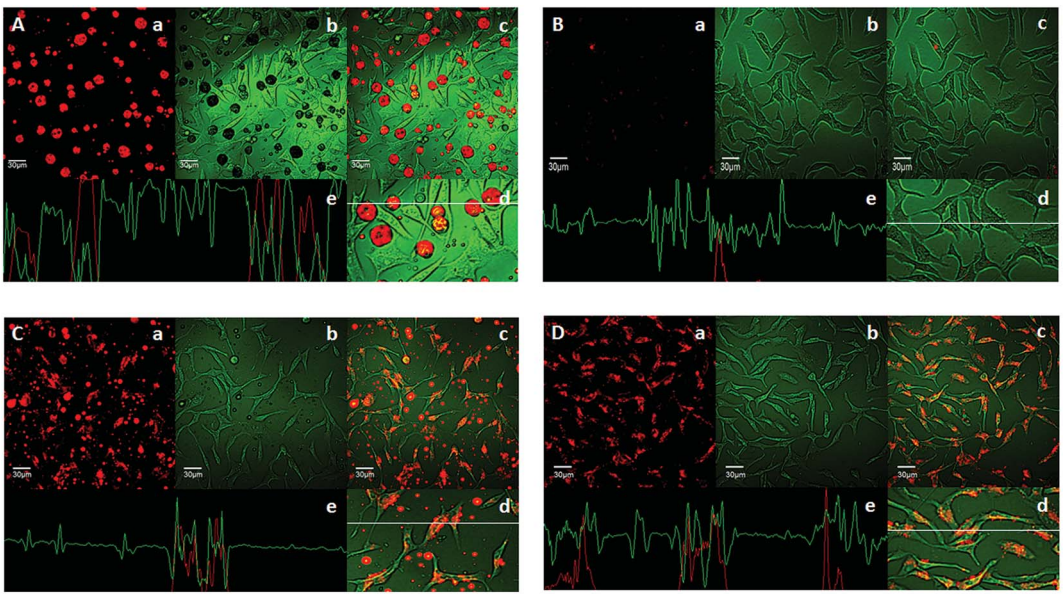

Fig. 11 Macrophage uptake of VLPP (A and B) and non-porous microparticles (C and D) before and after washing with HBSS (5×) respectively. In all the images, (a) red fluorescence images of microparticles; (b) transmission images (green) of macrophages and (c) superimposition of (a) and (b). (d) and (e) in all the images show line series analysis of fluorescence along the white line.

over a period of 7 days. VRZ was released at faster rate from porous microspheres compared to the non-porous microspheres. A biphasic release profile of VRZ was observed from all the formulations. The release of VRZ from the optimised VLPP was found to follow weibull release kinetics (Fig. 9B).

3.6 Safety studies

Dose response cytotoxicity profile of VRZ (1.2 nM to 150 μM) and VLPP (1.2 nM to 15 μM) were investigated to establish initial safety profile (Fig. 10A and B). The viability of cells was calculated with reference to the untreated cells where average absorbance was normalised to 100% viability. Cell viability results showed both VRZ and VLPP did not compromise cell viability and more than 90% of cells were viable following treatment with the highest concentration tested (100 μM for VRZ and 10 μM for VLPP, respectively).

Basolateral media collected after 4 h exposure to the VRZ and VLPP were analysed for the inflammatory marker, IL-8 (Fig. 10C). No significant increase in the level of secretion was observed ($p > 0.05$).

3.7 Phagocytic uptake of microparticles

Fraction of formulations collected from ACI stages 3 through 6 correspond to particles which may deposit from trachea to alveoli. As expected, the highly porous large particles were not taken up by macrophages in 3 h even though macrophages were found to be adherent to these particles (Fig. 11A). Following washing with HBSS (5×), most of the VLPP were removed as indicated by loss of red florescence. Further, line series analysis of fluorescence along the white line (Fig. 11B–d and e) demonstrated non-overlapping of green and red fluorescence, leading to the conclusion that macrophages were not able to engulf the highly porous particles. However, it is worthy to note that some florescent signals were still seen in the macrophages even after washing with HBSS (Fig. 11B).

On the other hand, most of non-porous particles were engulfed by the macrophages in 3 h (Fig. 11C and D). Following washing with HBSS (5×), small proportion of large non-porous particles not engulfed by macrophages (Fig. 11C) were removed and majority of non-porous particles were retained within the macrophages (Fig. 11D). In addition, line series analysis of fluorescence along the white line (Fig. 11D–d and e) demonstrated co-localisation of green and red fluorescence which suggested macrophages were able to engulf the non-porous particles.

4. Discussion

Sustained local effect of the drug in the lungs is mainly limited by the rapid absorption in the systemic circulation as well as phagocytic clearance of the drug delivery vehicle.[23] In order to achieve sustained delivery of VRZ in the lungs, highly porous microparticles of biodegradable polymers loaded with VRZ were formulated and extensively characterised for their biopharmaceutical characteristics desirable for efficient lung delivery.

QbD, in association with PCA, provided significant insights into the role played by various factors and their higher order interactions in determining the desirable CQAs of VLPP. I-optimal design was chosen since it allows the evaluation of categorical as well as numeric factors simultaneously while retaining the orthogonality of the design.[34] It is important to fit the design to the experiment and not the experiment to the design. I-optimal designs also offer advantage over D-optimal designs in terms of better predictability of response parameters.[34] PCA indicated that homogenization speed (PC1) and porogen concentration (PC2) were the most influential factors affecting the VLPP characteristics and must be closely monitored. Variables such as geometric diameter, span, AD and GSD of VLPP were found to be strongly dependent on the homogenization speed as indicated by high numerical score on the component 1 axis and were negatively correlated to the homogenization speed (Fig. 4 and 5). High homogenization speed led to the breakage of double emulsion into globules of smaller size resulted in VLPP with small particle size and narrow size distribution. Two-way interaction of homogenization speed and porogen concentration also played a role in determining the effective particle size of VLPP. Increase in homogenization speed led to decrease particle size of VLPP while increase in porogen concentration resulted in VLPP with larger geometric diameter as also evident from other studies.[35] Thus, the effective particle size of VLPP was mainly determined by the combination of porogen concentration and homogenization speed.

Efficient delivery of drug to the alveoli can be obtained by designing inhaled formulations with aerodynamic diameter between 1–5 μm.[36] It is further well documented that reduction in particle density led to decrease in aerodynamic diameter (as given by eqn (3)), while still retaining the large geometric diameter.[23] Addition of ammonium bicarbonate as effervescent porogen in the polymer phase as internal aqueous core was an effective way of forming highly porous large microparticles.[22] As expected, increase in the porogen concentration resulted in VLPP with increased pore size and pore density demonstrated by morphological examination by SEM (Fig. 6). In case of PLGA 502, broken VLPP were observed at high concentration of porogen. This may be because of less inherent strength of PLGA 502 which was unable to maintain integrity of the particles owing to highly porous structures. AFM imaging of the DoE model validation batches further revealed important nanoscopic characteristics of the optimised VLPP (Fig. 7). Post image analysis of AFM data revealed increase in surface roughness in case of porous particles as compared to non-porous particles (Table 5). This may be primarily because of the change in morphology of VLPP as a result of effervescence produced by ammonium bicarbonate during solidification process. Increased pore density with increased porogen concentration also resulted in concomitant decrease in the density and hence, increased porosity of the VLPP (Table 3).

Solid state characterisation of the VLPP demonstrated the absence of any crystalline VRZ within the VLPP as indicated by absence of melting endotherm and diffraction peaks of VRZ in the DSC thermogram and XRD spectra respectively (Fig. 3). Presence of amorphous form of VRZ is the indication of its stabilization in the presence of PLGA/PLA.

Complex relationships were found between the formulation and process factors and the *in vitro* aerosolisation performance of VLPP. This is evident by the DoE results (Table 3) as no single factor found to have significant influence on aerodynamic characteristics of VLPP. Complex interplay of process and formulation factors such as two way interactions, homogenization speed/porogen concentration and polymer type/porogen concentration influenced the aerodynamic characteristics of VLPP.

It was envisaged that the knowledge of work of cohesion and surface energetics operating within VLPP would be useful in fundamental understanding of the process of VLPP aerosolisation and dispersibility. Contact angle is a useful indicator of wettability, providing valuable information about surface energy using Lifshitz–van der Waals/acid–base approach.[22] Sessile drop contact angle method is the commonly applied methodology to study the surface of compact discs. However, numerous reports have been published which revealed that compaction leads to alteration of surface morphology and hence surface free energy of powders.[37] In the present study, the contact angle was determined by adhering powder to the inert support, thus allowing evaluation of surface characteristics of the powders as such without alteration. Particulate interactions at the surface include electrostatic, capillary forces and van der Waals (proximity) forces as well as mechanical interlocking.[24] Complexities are further increased by presence of amorphous domains on the particle surface, impurities present and specific polar/non-polar region (dispersive, acid/base surface energetics).[24,38] Hence, establishing direct correlations between such complex interplay of forces and the dispersibility/aerosolisation characteristics is difficult to achieve experimentally, although it seems convincible to achieve this on theoretical principles. Interestingly, a positive correlation ($R^2 = 0.825$) was observed between the FPF and the surface free energy of VLPP (Fig. 8). With the increase in surface energy of VLPP, aerosolisation performances were found to improve as indicated by increase in FPF. This is counterintuitive to the generally held notion that increase in surface energy promotes particle adhesion and hence hinders efficient particle dispersion. A possible explanation for such paradoxical correlation could be explained by considering the effect of aerodynamic drag exerted on the agglomerates as elucidated by following two eqn (7) and (8).

$$F_{\text{drag}} = C_{\text{d}}\frac{\pi}{8}\rho_{\text{air}}{\Phi_{\text{agg}}}^2{v_{\text{flow}}}^2 \quad (7)$$

$$E_{\text{c}}^{\ t_0} = C_{\text{d}}\frac{\pi}{12}\rho_{\text{agg}}\left({\Phi_{\text{agg}}}^{t_0}\right)^3{v_{\text{flow}}}^2 \quad (8)$$

where C_{d} is the drag coefficient, which is dependent on the ratio of inertial and frictional forces of the agglomerated particles in the airflow, ρ_{air} is the density of the air, Φ_{agg} is the effective diameter of the agglomerate, v_{flow} is the airflow velocity, ρ_{agg} is the density of the agglomerate. F_{drag} and E_{c} represent the aerodynamic drag acted and initial kinetic energy experienced by the particle agglomerate.

These equations clearly express that aerodynamic drag acting on the particles and the kinetic energy experienced by the agglomerate is directly proportional to the square and cubic of its diameter respectively. Hence, large loose aggregates formed as a result of increased cohesive forces due to higher surface energy experienced greater shear resulting in efficient de-agglomeration and hence increase in FPF. Similar results have also been obtained in some previous studies.[38,39]

Porosity of the VLPP governed the amount of VRZ released at the initial stage and the cumulative amount of drug released within 7 days (Fig. 9). Maximum release of VRZ was obtained in case of porous particles formulated with 5% porogen concentration as compared to VLPP formulated with 3% porogen concentration and non-porous particles. In comparison to sustained release of drugs for weeks from PLGA microspheres/nanospheres, a faster release of VRZ was observed in all the VLPP formulations. This might be due to solubility of VRZ (0.7 mg mL^{-1}) in water and porous network within the VLPP which resulted in faster release of VRZ from VLPP.

The A549 cell viability and determination of inflammatory marker (IL-8) studies established initial safety of VRZ and VLPP (Fig. 10). These results also support the findings of the toxicity studies of inhaled VRZ solution in rats carried by Tolman *et al.*[40] However, extensive *in vivo* toxicity studies are needed to be carried out to establish the long term safety of VLPP.

Uptake studies of VLPP in murine macrophages clearly demonstrated that VLPP was large enough to evade macrophage uptake and thus, ensuring prolonged residence at the site of infection (Fig. 11A). In fact, we and others have reported earlier that particles of ~8–12 μm show very little or no uptake by macrophages, while significantly greater uptake is observed with 1–5 μm particles.[20,22,41,42] The slight red florescence observed after washing of macrophages with HBSS (5×) (Fig. 11B) were most likely to be due to fragments of VLPP. However, the fraction of VLPP engulfed by macrophages was relatively small as indicated by little red florescence and its contribution to the total drug loss is expected to be insignificant. Non-porous particles, on the other hand, in the size range of 1–5 μm particles were significantly engulfed by macrophages which may constitute major portion of total drug loss (Fig. 11C and D).

Although the results demonstrate suitability of VLPP for the pulmonary delivery of VRZ, the major limitation of using large low density particles may be the increased bulk of powder to achieve therapeutically relevant dose. However, it is worth to mention that drug powder inhalers are a combination product requiring a drug formulation and device. Recently, a new inhaler device Orbital® has been designed to deliver high doses (hundreds of milligrams) of drug to the respiratory tract *via* multiple inhalation manoeuvres.[43] Development of such devices and combining them with efficient formulations can deliver high doses of drugs such as antibiotics and antifungals to treat the infections of the lungs.

5. Conclusion

Inhaled monotherapy of VRZ as polymeric dry powder represents an attractive option for the targeted treatment of IPA. In order of achieve sustained delivery of VRZ in the lungs, VLPP were prepared and optimised using QbD principles. VLPP prepared from PLA were able to meet desirable CQAs for lung delivery in terms of physiochemical characteristics as well safety profile and macrophage uptake. Animal studies are required to

further evaluate the sustained delivery of VRZ and safety following pulmonary administration of VLPP.

Acknowledgements

Authors are thankful to Director, NIPER for providing necessary infrastructure facilities and for financial support.

References

1 T. F. Patterson, *Lancet*, 2005, **366**, 1013–1025.
2 P. Venkatesan, J. R. Perfect and S. A. Myers, *Dermatol. Ther.*, 2005, **18**, 44–57.
3 T. J. Walsh, E. J. Anaissie, D. W. Denning, R. Herbrecht, D. P. Kontoyiannis, K. A. Marr, V. A. Morrison, B. H. Segal, W. J. Steinbach, D. A. Stevens, J. A. van Burik, J. R. Wingard and T. F. Patterson, *Clin. Infect. Dis.*, 2008, **46**, 327–360.
4 D. Sheppard and L. M. Grist, *Future Microbiol.*, 2010, **5**, 1001–1004.
5 P. Chandrasekar, *Eur. J. Haematol.*, 2010, **84**, 281–290.
6 M. Karthaus and D. Buchheidt, *Curr. Pharm. Des.*, 2013, **19**, 3569–3594.
7 O. Hilberg, C. U. Andersen, O. Henning, T. Lundby, J. Mortensen and E. Bendstrup, *Eur. Respir. J.*, 2012, **40**, 271–273.
8 G. F. Behre, S. Schwartz, K. Lenz, W. D. Ludwig, H. Wandt, E. Schilling, V. Heinemann, H. Link, A. Trittin and O. Boenisch, *et. al.*, *Ann. Hematol.*, 1995, **71**, 287–291.
9 C. A. Alvarez, N. P. Wiederhold, J. T. McConville, J. I. Peters, L. K. Najvar, J. R. Graybill, J. J. Coalson, R. L. Talbert, D. S. Burgess, R. Bocanegra, K. P. Johnston and R. O. Williams 3rd, *J. Infect.*, 2007, **55**, 68–74.
10 I. Bekersky, G. W. Boswell, R. Hiles, R. M. Fielding, D. Buell and T. J. Walsh, *Pharmaceut. Res.*, 2000, **17**, 1494–1502.
11 Z. Erjavec, G. M. Woolthuis, H. G. de Vries-Hospers, W. J. Sluiter, S. M. Daenen, B. de Pauw and M. R. Halie, *Eur. J. Clin. Microbiol. Infect. Dis.*, 1997, **16**, 364–368.
12 J. Gavalda, M. T. Martin, P. Lopez, X. Gomis, J. L. Ramirez, D. Rodriguez, O. Len, Y. Puigfel, I. Ruiz and A. Pahissa, *Antimicrob. Agents Chemother.*, 2005, **49**, 3028–3030.
13 E. J. Ruijgrok, A. G. Vulto and E. W. Van Etten, *J. Pharm. Pharmacol.*, 2000, **52**, 619–627.
14 J. M. Vaughn, N. P. Wiederhold, J. T. McConville, J. J. Coalson, R. L. Talbert, D. S. Burgess, K. P. Johnston, R. O. Williams 3rd and J. I. Peters, *Int. J. Pharm.*, 2007, **338**, 219–224.
15 J. A. Tolman, N. A. Nelson, Y. J. Son, S. Bosselmann, N. P. Wiederhold, J. I. Peters, J. T. McConville and R. O. Williams 3rd, *Eur. J. Pharm. Biopharm.*, 2009, **72**, 199–205.
16 N. A. Beinborn, H. L. Lirola and R. O. Williams 3rd, *Int. J. Pharm.*, 2012, **429**, 46–57.
17 N. A. Beinborn, J. Du, N. P. Wiederhold, H. D. Smyth and R. O. Williams 3rd, *Eur. J. Pharm. Biopharm.*, 2012, **81**, 600–608.
18 B. Sinha, B. Mukherjee and G. Pattnaik, *Nanomed. Nanotech. Biol. Med.*, 2013, **9**, 94–104.
19 B. Patel, N. Gupta and F. Ahsan, *J. Aerosol Med. Pulm. Drug Delivery*, 2014, **27**, 12–20.
20 B. Patel, V. Gupta and F. Ahsan, *J. Controlled Release*, 2012, **162**, 310–320.
21 F. Ungaro, C. Giovino, C. Coletta, R. Sorrentino, A. Miro and F. Quaglia, *Eur. J. Pharm. Sci.*, 2010, **41**, 60–70.
22 Y. Yang, N. Bajaj, P. Xu, K. Ohn, M. D. Tsifansky and Y. Yeo, *Biomaterials*, 2009, **30**, 1947–1953.
23 D. A. Edwards, J. Hanes, G. Caponetti, J. Hrkach, A. Ben-Jebria, M. L. Eskew, J. Mintzes, D. Deaver, N. Lotan and R. Langer, *Science*, 1997, **276**, 1868–1871.
24 E. Oh and P. E. Luner, *Int. J. Pharm.*, 1999, **188**, 203–219.
25 S. Jain, D. Kumar, N. K. Swarnakar and K. Thanki, *Biomaterials*, 2012, **33**, 6758–6768.
26 H. Lin, H. Li, H. J. Cho, S. Bian, H. J. Roh, M. K. Lee, J. S. Kim, S. J. Chung, C. K. Shim and D. D. Kim, *Journal of pharmaceutical science*, 2007, **96**, 341–350.
27 S. M. Hwang, D. D. Kim, S. J. Chung and C. K. Shim, *J. Controlled Release*, 2008, **129**, 100–106.
28 Z. Zsengeller, K. Otake, S. A. Hossain, P. Y. Berclaz and B. C. Trapnell, *J. Virol.*, 2000, **74**, 9655–9667.
29 S. Wold, P. Geladi, K. Esbensen and J. Öhman, *J. Chemom.*, 1987, **1**, 41–56.
30 W. Dunn Iii, D. Scott and W. Glen, *Tetrahedron Comput. Methodol.*, 1989, **2**, 349–376.
31 X. Teng, J. Ren and S. Gu, *J. Biomed. Mater. Res., Part B*, 2007, **81**, 185–193.
32 H. K. Kim, H. J. Chung and T. G. Park, *J. Controlled Release*, 2006, **112**, 167–174.
33 M. J. Kwon, J. H. Bae, J. J. Kim, K. Na and E. S. Lee, *Int. J. Pharm.*, 2007, **333**, 5–9.
34 B. Jones and P. Goos, *I-optimal versus D-optimal split-plot response surface designs*, 2012.
35 L. X. Yu, *Pharmaceut. Res.*, 2008, **25**, 781–791.
36 B. Forbes, B. Asgharian, L. A. Dailey, D. Ferguson, P. Gerde, M. Gumbleton, L. Gustavsson, C. Hardy, D. Hassall, R. Jones, R. Lock, J. Maas, T. McGovern, G. R. Pitcairn, G. Somers and R. K. Wolff, *Adv. Drug Delivery Rev.*, 2011, **63**, 69–87.
37 F. Fichtner, D. Mahlin, K. Welch, S. Gaisford and G. Alderborn, *Pharmaceut. Res.*, 2008, **25**, 2750–2759.
38 P. Begat, D. A. Morton, J. N. Staniforth and R. Price, *Pharmaceut. Res.*, 2004, **21**, 1826–1833.
39 R. Salama, S. Hoe, H. K. Chan, D. Traini and P. M. Young, *Eur. J. Pharm. Biopharm.*, 2008, **69**, 486–495.
40 J. A. Tolman, N. A. Nelson, S. Bosselmann, J. I. Peters, J. J. Coalson, N. P. Wiederhold and R. O. Williams 3rd, *Int. J. Pharm.*, 2009, **379**, 25–31.
41 C. Thomas, V. Gupta and F. Ahsan, *Pharmaceut. Res.*, 2010, **27**, 905–919.
42 D. A. Edwards, A. Ben-Jebria and R. Langer, *J. Appl. Physiol.*, 1998, **85**, 379–385.
43 P. M. Young, J. Crapper, G. Philips, K. Sharma, H. K. Chan and D. Traini, *J. Aerosol Med. Pulm. Drug Delivery*, 2014, **27**, 138–147.